

# Study on Hydroxylammonium-Based Ionic Liquids. II. Computational Analysis of CO<sub>2</sub> Absorption

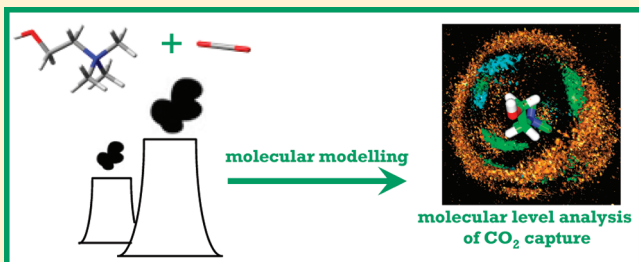
Santiago Aparicio,<sup>\*,†</sup> Mert Atilhan,<sup>‡</sup> Majeda Khraisheh,<sup>‡</sup> Rafael Alcalde,<sup>†</sup> and Javier Fernández<sup>‡</sup>

<sup>†</sup>Department of Chemistry, University of Burgos, 09001 Burgos, Spain

<sup>‡</sup>Chemical Engineering Department, Qatar University, Doha, Qatar

 Supporting Information

**ABSTRACT:** In the previous work of this series, we reported a wide experimental and computational analysis of the properties of hydroxylammonium-based ionic liquids. This family of ionic liquids shows very favorable economical, technological, and environmental properties in comparison with other ionic liquid types. We report in this work a computational study, using quantum chemistry and molecular dynamics methods, to analyze the absorption of carbon dioxide by hydroxylammonium ionic liquids. The selected compounds were 2-hydroxyethyl-trimethylammonium L-(+)-lactate and tris(2-hydroxyethyl)methylammonium methylsulfate. The main objective of this work is to study and analyze CO<sub>2</sub> absorption from the molecular point of view, therefore contributing to the knowledge and advancement on the absorption ability of ionic liquids. The computational study would lead to a deeper knowledge of factors controlling CO<sub>2</sub> absorption for this ionic liquid family in comparison with available information for other relevant types. The results were analyzed considering the effects of absorbed gas on the ionic liquid structuring from a molecular level viewpoint, interionic interactions, diffusion of the involved compounds, and interaction of CO<sub>2</sub> with anions and cations. The reported results show a strong effect of the presence of hydroxyl groups in the involved cations and anions through the interaction with CO<sub>2</sub> molecules, along with the effects rising from the size of cations on the fluid structure.



## 1. INTRODUCTION

There is a growing belief that global climate change is occurring, and although it is not a proven fact, many climate scientists consider that a major cause for this change is anthropogenic emission of greenhouse gases (GHGs) into the atmosphere.<sup>1</sup> The most released GHG is carbon dioxide, and for this gas, the most important sources are energy-intensive related emissions. Hence, approximately 25% of the total CO<sub>2</sub> emissions in the world are produced from combustion and nonfuel uses of fossil fuels for electricity generation.<sup>2</sup> Moreover, world CO<sub>2</sub> energy related emissions are projected to increase at a 2.1% rate per year,<sup>3</sup> which is in agreement with the forecasted consumption of fossil fuels for electricity generation.<sup>3</sup> Since renewable sources will not be sufficient to supply the required energy in the coming years, fossil fuels will remain the major source for electricity generation and supply. Hence, to control CO<sub>2</sub> emissions from these sources will be extremely important to minimize GHG contributions to climate change without stifling economical and technological development. The available alternatives for carbon dioxide emissions from the combustion of fossil fuels for electricity production require CO<sub>2</sub> capture from sources where it is formed through (i) postcombustion, (ii) precombustion, or (iii) oxy-fuel methods.<sup>4</sup> Postcombustion treatment is the most suitable option, mainly because it may be applied to most of the existing fossil fuel powered plants.<sup>4</sup> The current technologies

used for CO<sub>2</sub> capture are amine based and its derivatives methods, in which a chemical absorption of CO<sub>2</sub> is produced.<sup>5</sup> Using these amine-based methods, CO<sub>2</sub> may be removed to low levels from mixed gases at low partial pressure, as in flue gases, but the capturing ability of these methods is limited by equilibrium. Nevertheless, amine absorption methods have numerous technological problems,<sup>6,7</sup> and thus, new methods are required.

Ionic liquids have attracted great attention since they are considered possible candidates for CO<sub>2</sub> capture and emission reduction,<sup>8,9</sup> and thus, different types of ionic liquids have been studied.<sup>10,11</sup> We reported in a recent review work the state-of-the-art studies on the absorption of CO<sub>2</sub> using ionic liquids, leading to the conclusion that ionic liquids are promising fluids for CO<sub>2</sub> absorption processes due to their unique characteristics, yet further studies have to be performed to reach suitable alternatives to current processes.<sup>10</sup> One of the most important aspects for advancing the CO<sub>2</sub> capturing technology using ionic liquids is the accurate knowledge of the molecular level factors controlling the gas absorption. A deep knowledge of the absorption process may be obtained using advanced computational chemistry tools, which allow us to infer (i) the mechanism of

**Received:** July 1, 2011

**Revised:** August 30, 2011

**Published:** September 20, 2011

absorption, (ii) the effect of the absorbed gas on the ionic liquid structure and properties, and (iii) the relationship between ionic liquid structure and molecular-level properties with the gas absorption ability, thus allowing us to develop structure–property relationships. The large number of possible anion–cation combinations leading to ionic liquids hinders experiment with all of them because of the costly, both in time and resources, absorption measurements, and thus, the computational approach would allow directing experimental studies in the right direction, reducing the possible candidates. Therefore, several relevant aspects have been analyzed using a molecular simulation approach such as the partial molar volume of CO<sub>2</sub> in ionic liquids,<sup>12</sup> viscosity variation with CO<sub>2</sub> absorption,<sup>13</sup> solvation of CO<sub>2</sub> in ionic liquids,<sup>14</sup> molecular level structural aspects,<sup>15</sup> or the development of computational tools for predicting CO<sub>2</sub> solubility.<sup>16</sup>

We report computational analysis of CO<sub>2</sub> absorption on two selected hydroxylammonium-based ionic liquids, 2-hydroxyethyl-trimethylammonium L-(+)-lactate ([HE3MA]LAC) and tris(2-hydroxyethyl)methylammonium methylsulfate ([3HEMA]MS), in this work. These ionic liquids were selected based on two main reasons: (i) their remarkably adequate environmental, toxicological, and low cost properties and (ii) the presence of functional groups such as hydroxyl, carboxylate, and sulfate that may lead to complex interactions both between the involved ions together with CO<sub>2</sub> absorbed molecules. In a previous work,<sup>17</sup> we analyzed the properties of these ionic liquids from experimental studies and atomistic simulations, and we extend the study to the analysis of CO<sub>2</sub> absorption using computational tools. We will use three computational tools to analyze the studied systems: (i) quantum chemistry methods to analyze short-range interactions between CO<sub>2</sub> molecules and the involved ions, (ii) a COSMO-RS<sup>18</sup> approach to predict gas solubility from quantum chemistry results, and (iii) molecular dynamics atomistic simulations to analyze the absorption process from structural, energetic, and dynamic viewpoints. Therefore, the reported results would lead to a molecular level understanding of the CO<sub>2</sub> absorption process in the studied ionic liquids.

## 2. SIMULATION DETAILS

A computational methodology was described in detail in previous work;<sup>17</sup> therefore, we will describe only the main aspects of computational tools in this work. Quantum chemistry calculations were done with the density functional theory (DFT) approach by using the Gaussian 03 package.<sup>19</sup> The Becke gradient-corrected exchange functional<sup>20</sup> and Lee–Yang–Parr correlation functional<sup>21</sup> with three parameters (B3LYP)<sup>22</sup> method together with a 6-311++g\*\* basis set were used in this work. Atomic charges were calculated to fit the electrostatic potential<sup>23</sup> according to the Merz–Singh–Kollman (MK)<sup>24</sup> scheme. Interaction energies for complexes,  $\Delta E$ , were calculated as the differences among the complex and sum of monomers' energies at the same theoretical level, with basis set superposition error (BSSE) corrected through the counterpoise procedure.<sup>25</sup> Atoms in a molecule (AIM) calculations<sup>26</sup> were carried out using the AIM2000 program<sup>27</sup> to get a deeper insight into anion/cation/CO<sub>2</sub> interactions.

COSMO-RS calculations were done with the COSMOthermX program for structures optimized in the Gaussian 03 package at the B3LYP/6-311++g\*\* level. For these structures, COSMO files were calculated at the BVP86/TZVP/DGA1 level and used for all the

calculations. The model parametrization used for all the physicochemical COSMO calculations was BP\_TZVP\_C21\_0111.

Classical molecular dynamics simulations were carried out using the MDynaMix v. 5.0 molecular modeling package.<sup>28</sup> Molecular dynamics was analyzed to infer structural, energetic, and dynamic properties of the studied fluids. Simulations were performed in the NPT ensemble using the Nose–Hoover method to control the temperature and pressure of the simulation system.<sup>29</sup> The equations of motion were solved by the Tuckerman–Berne double time step algorithm,<sup>30</sup> with long and short time steps of 1 and 0.1 fs, respectively. The Ewald summation method<sup>31</sup> was implemented for the Coulombic interactions with a radius cutoff of 1.5 nm. The simulated systems consist of cubic boxes of pure ionic liquids or ionic liquids with absorbed CO<sub>2</sub>, with the compositions reported in Table S1 (Supporting Information). Initial boxes were generated placing randomly ions and CO<sub>2</sub> molecules in an FCC lattice at low density ( $\sim$ 0.2 to 0.3 g cm<sup>-3</sup>), and then NPT simulations were performed at the selected pressure and temperature to ensure equilibration, which is checked through constant potential energy. After equilibration, 10 ns runs (time step 1 fs) in the NPT ensemble at the studied pressure and temperature were performed for the analysis of systems' properties. Force field parametrization for ionic liquids and validation was reported in the previous work,<sup>17</sup> and parameters for CO<sub>2</sub> molecules were obtained from the literature.<sup>15</sup>

## 3. RESULTS AND DISCUSSION

**3.1. COSMO Predictions.** The COSMO-RS method is a thermodynamic model based on quantum chemistry calculations that have been used in the literature for the prediction of CO<sub>2</sub> solubility in ionic liquids,<sup>32</sup> mainly for screening purposes.<sup>33,34</sup> The available studies on the predictive ability of the COSMO-RS model for gas solubilities in ionic liquids have proven to be successful; Ab-Manan et al.<sup>32</sup> reported a relative absolute deviation of 36.9 % for 27 ionic liquids. Therefore, this approach could assist in qualitative ranking of the CO<sub>2</sub> solubility in the selected hydroxylammonium-based ionic liquids.

We report in Figure 1  $\sigma$ -surfaces (screening charge density, which are opposed by definition to molecular charge distribution) and  $\sigma$ -profiles (histograms of screening charge) for the ions studied in this work.<sup>35</sup> For the [HE3MA] cation,  $\sigma$ -surfaces show positive values (red areas) corresponding to the hydroxyl oxygens and negative values (blue areas) corresponding to hydroxyl hydrogens. The  $\sigma$ -profile may be analyzed considering the cutoff values for the hydrogen bond donor region ( $\sigma < 0.009 \text{ e } \text{\AA}^{-2}$ ) and hydrogen bond acceptor region ( $\sigma > 0.009 \text{ e } \text{\AA}^{-2}$ ), and the values reported in Figure 1a for the [HE3MA] cation show several peaks (hot spots) in both regions corresponding to the cationic hydroxyl atoms. For the [3HEMA] cation, these effects in the hydrogen bonding donor–acceptor regions are reinforced as we see in Figure 1c. In the case of the LAC anion,  $\sigma$  values show a remarkable peak in the hydrogen bond acceptor region at 0.018 corresponding to the hydroxyl and carboxylate oxygens, whereas no remarkable peaks appear in the hydrogen bonding donor region (negative values). For the MS anion, a strong and sharp peak appears at 0.015 corresponding to the hydrogen bonding acceptor sites placed in the oxygens from the large red region plotted in the corresponding  $\sigma$ -surface. Therefore, these ions are characterized by the presence of remarkable hotspots in the hydrogen bond donor and acceptor

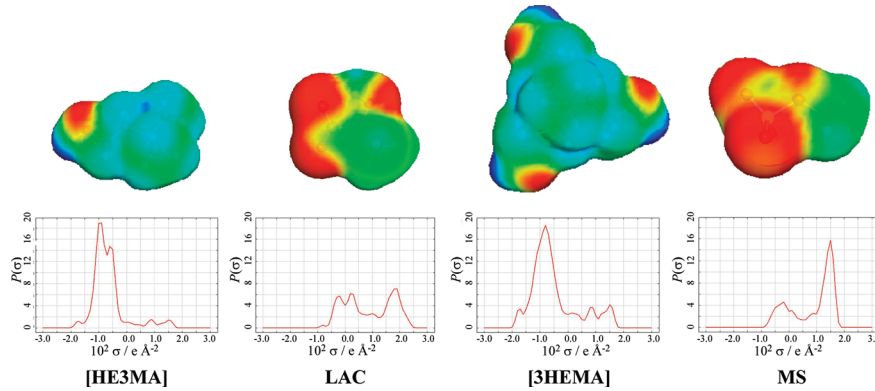


**Figure 1.**  $\sigma$ -Surfaces (screening charge density, top) and  $\sigma$ -profiles (histograms of screening charge distribution, bottom) for the ions studied in this work. Color code for panel (a): from positive screening charges (electrostatically negative) in red to negative screening charges (electrostatically positive) in blue.

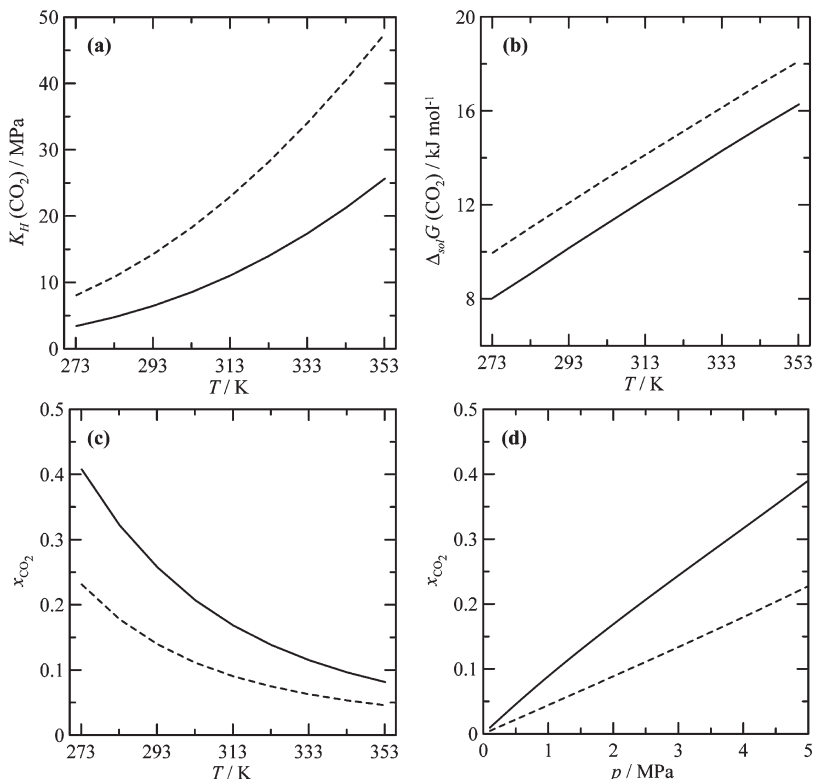


**Figure 2.** Results of COSMOthermX calculations for (continuous lines) [HE3MA]LAC (dashed lines) and [3HEMA]MS. (a) Henry's law constant,  $K_H$ . (b) Gibbs energy of solvation,  $\Delta_{\text{sol}}G$ , and gas solubility ( $\text{CO}_2$  mole fraction,  $x_{\text{CO}_2}$ ) as a function of (c) temperature ( $p = 2.5$  MPa) and (d) pressure ( $T = 303.15$  K).

regions, which correspond to highly polarized molecules: hydroxyl ammonium cations with strong hydrogen bond donor/acceptor regions and anions mainly with strong hydrogen bonding acceptor regions. These results are in agreement with the high polarity inferred for these ionic liquids using other approaches reported in the previous work of this series.<sup>17</sup> Hence, anion–cation interaction and ion–CO<sub>2</sub> interaction will be strongly affected by this ionic polarity.

The calculated screening charge density is the key property for the prediction of thermodynamic properties for the studied systems using the COSMO-RS approach. We have used the method to predict CO<sub>2</sub> solubility as reported in Figure 2. Henry's

law constant,  $K_H$ , is reported in Figure 2a for both ionic liquids as a function of temperature, being lower for [HE3MA]LAC than for [3HEMA]MS. Nevertheless, both ionic liquids show moderate CO<sub>2</sub> absorption ability, and predicted  $K_H$  values at 298.15 K are 7.5 and 16.2 MPa for [HE3MA]LAC and [3HEMA]MS, respectively, which are larger than the values reported by Zhang et al.<sup>33</sup> for several families of ionic liquids using also the COSMO-RS approach. The effect of hydroxylammonium cations seems to have a remarkable effect on the CO<sub>2</sub> solubility (decreasing it). Zhang et al.<sup>33</sup> reported  $K_H = 6.2$  and 5.0 for 1-butyl-3-methylimidazolium lactate and methylsulfate ionic liquids, respectively, and thus, when the imidazolium cation is replaced by hydroxylammonium

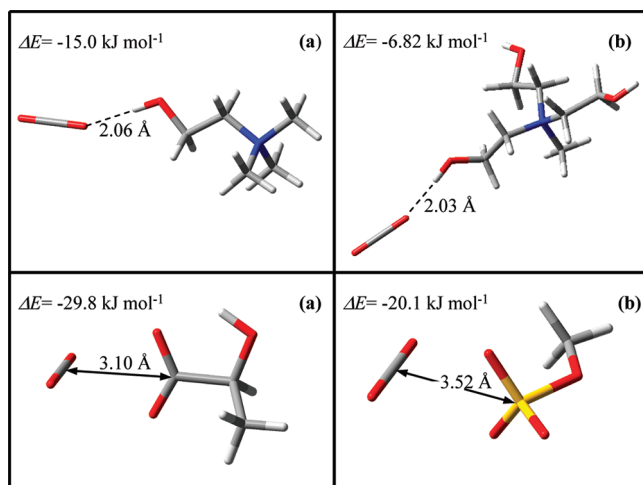


**Figure 3.**  $\text{CO}_2$ -ion complexes calculated at the B3LYP/6-311++g\* theoretical level.  $\Delta E$  stands for counterpoise corrected interaction energies. Arrows show relevant interatomic distances, and dashed lines in panels a and b show possible hydrogen bonds. Atom color code: (gray) carbon, (blue) nitrogen, (red) oxygen, (yellow) sulfur, and (light gray) hydrogen.

cations maintaining the anions  $K_H$  increases remarkably, especially for the bulky [3HEMA] cation. Nevertheless, we should remark that the objective of this work is to understand the underlying mechanism that controls  $\text{CO}_2$  solubility as a function of the involved ions rather than proposing candidates for  $\text{CO}_2$  capture agents. In a previous work, we analyzed the  $\text{CO}_2$  absorption behavior from a molecular viewpoint of guanidium-based ionic liquids containing lactate anions,<sup>36</sup> whereas in this work we would analyze the effect of hydroxylammonium cations. Therefore, the presence of hydroxyl groups in the cation seems to decrease  $\text{CO}_2$  solubility, which is a surprising effect because we could expect that  $\text{CO}_2$  molecules could interact effectively with these cationic hydroxyl groups and thus lead to stronger absorption. This behavior will be analyzed in detail in this work.

We have calculated the Gibbs energy of solvation,  $\Delta_{\text{sol}}G$ , for  $\text{CO}_2$  in both ionic liquids (Figure 2b); for these low pressures,  $\Delta_{\text{sol}}G$  may be considered a good approximation of Gibbs energy of solution.  $\Delta_{\text{sol}}G$  shows a similar trend with temperature for both ionic liquids, showing larger values for [3HEMA]MS. Enthalpy,  $\Delta_{\text{sol}}H$ , and entropy,  $\Delta_{\text{sol}}S$ , of solvation were calculated from the corresponding partial derivatives of  $\Delta_{\text{sol}}G$  with temperature.<sup>32</sup>  $\Delta_{\text{sol}}H$  is negative, exothermic solvation being more negative for [HE3MA]LAC; for example, at 298.15 K  $\Delta_{\text{sol}}H$  is  $-20.8$  and  $-18.5 \text{ kJ mol}^{-1}$  for [HE3MA]LAC and [3HEMA]MS, respectively.  $\Delta_{\text{sol}}H$  passes through a minimum with increasing temperature at around 300 K and increases for both ionic liquids. For  $\Delta_{\text{sol}}S$ , all the values are negative, more negative for [HE3MA]LAC, but differences between both ionic liquids are in the 1–2% range; for example,  $\Delta_{\text{sol}}S$  is  $-105.7$  and  $-104.3 \text{ J mol}^{-1} \text{ K}^{-1}$  for [HE3MA]LAC and [3HEMA]MS, respectively.  $\Delta_{\text{sol}}S$  evolves through less negative values with increasing temperature, passing through a minimum at around 300 K for both ionic liquids.  $\Delta_{\text{sol}}H$  may be related to the  $\text{CO}_2$ -ionic liquid molecular interactions and  $\Delta_{\text{sol}}S$  to the structuring of solvent molecules (ionic liquid) surrounding the solute ( $\text{CO}_2$ ),<sup>37</sup> and thus we may conclude stronger interactions between  $\text{CO}_2$  molecules and [HE3MA]LAC ionic liquid and a similar

structuring of the ionic liquid around the solute as the  $\Delta_{\text{sol}}S$  values show. Therefore, the hydroxylammonium cation plays a prevailing role in the  $\text{CO}_2$  absorption for these ionic liquids in comparison with the effect of LAC or MS anions. We report also in Figure 2c and d the effect of temperature and pressure on the  $\text{CO}_2$  solubility, and the reported results show again moderate  $\text{CO}_2$  solubility, almost double for [HE3MA]LAC than for [3HEMA]MS in the pressure–temperature ranges studied.

**3.2. Quantum Chemistry Calculations.** Calculations performed using the DFT approach at the B3LYP/6-311++g\*\* theoretical level were done to infer information about the ion– $\text{CO}_2$  short-range interactions. Structures for the optimized ion– $\text{CO}_2$  pairs are reported in Figure 3, and the absence of imaginary vibrational frequency confirms that these pairs correspond to true minima. The interaction of  $\text{CO}_2$  molecules with hydroxylammonium cations is performed through the hydroxyl groups, as we may have expected (Figures 3a and 3b), being more effective with [HE3MA] than with [3HEMA]. Remarkably short distances between the oxygen atoms in  $\text{CO}_2$  and the hydrogen in cation hydroxyl groups are obtained, thus pointing to an effective interaction. For the  $\text{CO}_2$ –anion interactions, we should remark that they are stronger than the corresponding  $\text{CO}_2$ –cation interactions. Interaction with the LAC anion is stronger than with the MS anion.  $\text{CO}_2$  molecules interact with the LAC anion through the COO position in a T-shaped way, and a similar interaction is obtained with MS but with  $\text{CO}_2$  molecules at longer distances. The results for LAC– $\text{CO}_2$  complexes are in fair agreement with those reported by Wang et al.<sup>38</sup> They reported  $-25.34 \text{ kJ mol}^{-1}$  interaction energy at B3LYP/6-311++g\*\*, which is 15% lower than the value reported in this work at the B3LYP/6-311++g\*\* level. Wang et al. also reported a bending of the  $\text{CO}_2$  molecule to reduce repulsive interactions leading to a  $167.5^\circ$  angle, and we have obtained in this work a value of  $170.7^\circ$  for the  $\text{CO}_2$  angle.  $\text{CO}_2$  oxygens are also bent outward when interacting with the MS anion, leading to a  $173.6^\circ$  angle. No bending is obtained for  $\text{CO}_2$  molecules interacting with [HE3MA] and [3HEMA] cations. In the case of a LAC– $\text{CO}_2$  interaction, a possible interaction could be proposed through the anion hydroxyl position, and we have analyzed several initial configurations for the optimization of LAC– $\text{CO}_2$  pair, some of them beginning from the  $\text{CO}_2$  molecule placed close to the LAC hydroxyl group. All of them led to the configuration reported in Figure 3c, and thus we may conclude that interaction with the COO group is clearly preferred, lower energy, than interaction through the hydroxyl group.

Sudha et al.<sup>39</sup> reported, for imidazolium-based ionic liquids, that anion– $\text{CO}_2$  interaction energies are inversely proportional to  $\text{CO}_2$  solubility, which would justify the moderate solubilities of  $\text{CO}_2$  in the ionic liquids studied in this work because of the relatively large anion– $\text{CO}_2$  interaction energies reported in Figure 3. Nevertheless, MS– $\text{CO}_2$  interaction energy is lower (in absolute value) than for LAC– $\text{CO}_2$ , and thus, according to Sudha et al., solubility in MS-containing ionic liquid should be larger, which is not true as the COSMO results reported in the previous section have shown. Therefore, cations should develop also a relevant role in  $\text{CO}_2$  absorption, especially for the hydroxylammonium-based ones studied in this work, for which the presence of hydroxyl groups leads to a moderately strong interaction with  $\text{CO}_2$  molecules.

To analyze the molecular origin and topological characteristics of the ion– $\text{CO}_2$  interactions, AIM analysis was performed for the optimized structures reported in Figure 3, and the main

results of the AIM approach are reported in Figure 4. For cation–CO<sub>2</sub> interactions a bond critical point (BCP) is obtained (Figure 3a and 3b); nevertheless, the electron density at BCP,  $\rho_{BCP}$ , and the Laplacian of electron density at BCP,  $\nabla^2_{BCP}$ , show moderate values for both cations. In the case of anion–CO<sub>2</sub> interactions, two BCPs and a ring critical point (RCP) are obtained both for LAC and MS anions. BCPs show lower  $\rho_{BCP}$  and  $\nabla^2_{BCP}$  for MS than for LAC, which would justify the lower interaction energies reported in Figure 3. Moreover,  $\rho_{BCP}$  and  $\nabla^2_{BCP}$  are low for both LAC and MS, but the presence of two BCPs and one RCP for each anion–CO<sub>2</sub> interaction would justify the stronger character of anion–CO<sub>2</sub> interactions in comparison with cation–CO<sub>2</sub> ones.

Ion–CO<sub>2</sub> interactions were also analyzed through the NBO approach by the second-order perturbation theory (Table 1). Three main properties are analyzed from the NBO approach to analyze the characteristics of the donor, *i*, acceptor, *j*, interaction: (i) second-order perturbation energy,  $E(2)$ , which is the stabilization energy from the *i* to *j* delocalization, (ii)  $\Delta E_{ij}$ , which is the energy difference between donor and acceptor, and (iii)  $F_{ij}$ , which is the off-diagonal Fock matrix element, which is related to

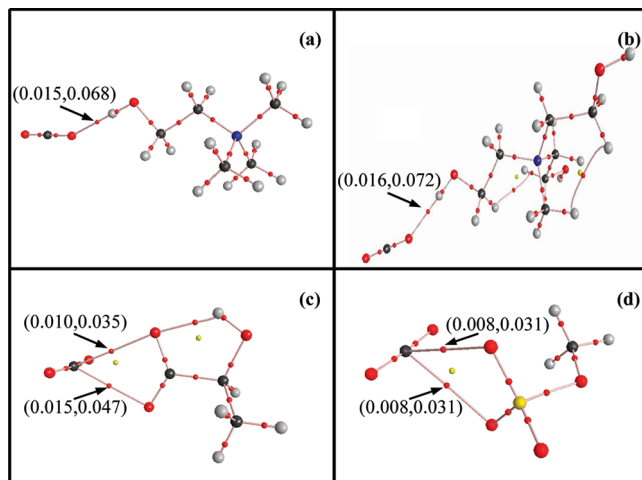


**Figure 4.** AIM analysis for CO<sub>2</sub>–ion complexes. Molecular graphs with small red dots representing bond critical points (BCP), small yellow dots representing ring critical points (RCP), pink lines representing bond paths, and large dots representing attractors (atoms: black, carbon; gray, hydrogen; red, oxygen; yellow, sulfur). Parenthesized values are shown for each relevant BCP (electron density at BCP, Laplacian of electron density, both in atomic units). Ring paths are not plotted for the sake of simplicity.

symmetry between the donor and acceptor. We have reported in Table 1 the most remarkable donor–acceptor interactions, largest stabilization energies, for the studied pairs. For the CO<sub>2</sub>–cation interactions, the reported results show that complexes are formed from the delocalization of oxygen lone pairs in CO<sub>2</sub> molecules toward  $\sigma^*$  in cation hydroxyl groups. Cation–CO<sub>2</sub> interactions through the first lone pair in CO<sub>2</sub> oxygens are remarkably more important than through the second lone pair, which may be justified considering the poor symmetry between the donor and acceptor for the second donor lone pair as the low  $F_{ij}$  values reported in Table 2 show. For the anion–CO<sub>2</sub> interaction, charge delocalization is produced from the lone pairs in COO oxygens for LAC or from SO<sub>3</sub> oxygens for MS toward the  $\sigma^*$  in CO<sub>2</sub>. Delocalization is more effective for CO<sub>2</sub>–LAC than for CO<sub>2</sub>–MS because of the lower symmetry between donor and acceptor orbitals (lower  $F_{ij}$  values) for MS. We should remark that  $\Delta E_{ij}$  values for cation–CO<sub>2</sub> are remarkably larger than for anion–CO<sub>2</sub>, but this last interaction is characterized by a poor symmetry, which leads to not too large  $E(2)$  values, especially for the CO<sub>2</sub>–MS pair.

**3.3. Molecular Dynamics Simulations.** Classical molecular dynamics simulations were done for  $x$  CO<sub>2</sub> + (1 –  $x$ ) ionic liquid mixtures with CO<sub>2</sub> mole fractions up to 0.4 (Table S1, Supporting Information), for isobaric (2.5 MPa) and isothermal (303 K) conditions. The larger CO<sub>2</sub> concentrations ( $x = 0.3$ –0.4) simulated in this work are clearly above the CO<sub>2</sub> solubility limit reported in previous sections for both ionic liquids, and thus they are simulations under supersaturated conditions.

**3.3.1. Volumetric Properties.** Huang et al.<sup>12</sup> showed that when CO<sub>2</sub> is absorbed in an ionic liquid its partial molar volume is remarkably lower than in common organic solvents, which was explained considering the sizes and shapes of the available cavities in the ionic liquids together with the rearrangement of these cavities upon absorption and the placement of CO<sub>2</sub> molecules in well-defined locations. We report in Figure 5a the molar volume for the studied CO<sub>2</sub> + ionic liquid mixtures, and the behavior obtained shows a linear decrease with increasing CO<sub>2</sub> mole fraction. We obtained a 29.4% and 31.1% decrease in molar volume for [HE3MA]LAC and [3HEMA]MS, respectively, when the CO<sub>2</sub> mole fraction evolves from 0 to 0.4. The calculated CO<sub>2</sub> partial molar volumes in both ionic liquids are low (Figure 5a), as we may have expected, being larger for the [3HEMA]MS ionic liquid. We reported in a previous work the volumetric properties of the CO<sub>2</sub> + hexamethylguanidinium lactate ([HMG]LAC) mixture leading to a CO<sub>2</sub> partial molar volume of 40.17 cm<sup>3</sup> mol<sup>-1</sup><sup>36</sup> which is slightly lower than the value obtained in this work for [HE3MA]LAC. Therefore,

**Table 1.** NBO Analysis of the Studied CO<sub>2</sub>–Ion Complexes Computed in the Gas Phase at the B3LYP/6-311++g\*\* Theoretical Level<sup>a</sup>

complex	donor	donor pair	acceptor	$E(2)$ /kJ mol <sup>-1</sup>	$\Delta E_{ij}$ /au	$F_{ij}$ /au
CO <sub>2</sub> –[HE3MA]	O (in CO <sub>2</sub> )	1	HO (in [HE3MA])	9.71	1.21	0.048
		2	HO (in [HE3MA])	2.85	0.75	0.022
CO <sub>2</sub> –[3HEMA]	O (in CO <sub>2</sub> )	1	HO (in [3HEMA])	10.80	1.22	0.050
		2	HO (in [3HEMA])	3.81	0.76	0.026
CO <sub>2</sub> –LAC <sup>b</sup>	O (in LAC –COO group)	2	CO (in CO <sub>2</sub> )	13.18	0.22	0.025
CO <sub>2</sub> –MS <sup>b</sup>	O (in MS –SO <sub>3</sub> group)	2	CO (in CO <sub>2</sub> )	3.89	0.25	0.014

<sup>a</sup> Second-order perturbation energy,  $E(2)$ , energy difference among the donor and the acceptor,  $\Delta E_{ij}$ , and Fock matrix element between the donor and the acceptor,  $F_{ij}$ . Values calculated for optimized structures reported in Figure 7. Reported values only for  $E(2) > 0.50$  kcal mol<sup>-1</sup>. <sup>b</sup> These interactions appear twice, one for each oxygen opposite to CO<sub>2</sub> molecules (Figure 1).

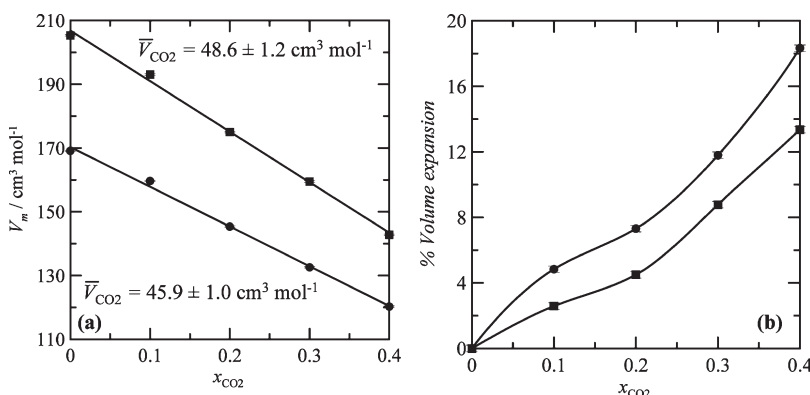
**Table 2.** Intermolecular Energy Contributions (Lennard-Jones, LJ, and Electrostatic, ELE) to the Liquid Phases of  $x \text{ CO}_2 + (1 - x)$  {[HE3MA]LAC or [3HEMA]MS} systems at 303 K/2.5 MPa Obtained from Molecular Dynamics Simulations<sup>a</sup>

$x \text{ CO}_2 + (1 - x)$ {[HE3MA]LAC}												
$x_{\text{CO}_2}$	A–A		A–C		C–C		A–CO <sub>2</sub>		C–CO <sub>2</sub>		CO <sub>2</sub> –CO <sub>2</sub>	
	LJ	ELE	LJ	ELE	LJ	ELE	LJ	ELE	LJ	ELE	LJ	ELE
0	-9.57	1307.96	-23.17	-3179.80	-19.79	1299.01	-	-	-	-	-	-
0.1	-8.70	1261.06	-22.20	-3066.48	-18.15	1236.67	-14.13	-2.81	-16.81	-6.77	-0.65	0.02
0.2	-8.22	1217.69	-21.32	-2989.90	-17.59	1209.30	-13.66	-5.00	-15.37	-9.10	-0.83	-0.64
0.3	-8.01	1171.22	-20.07	-2877.34	-16.77	1150.12	-13.00	-6.89	-14.63	-17.72	-1.28	-0.99
0.4	-7.30	1124.90	-18.39	-2750.22	-16.03	1074.57	-12.40	-8.75	-13.41	-20.12	-1.95	-0.92

$x \text{ CO}_2 + (1 - x)$ [3HEMA]MS												
$x_{\text{CO}_2}$	A–A		A–C		C–C		A–CO <sub>2</sub>		C–CO <sub>2</sub>		CO <sub>2</sub> –CO <sub>2</sub>	
	LJ	ELE	LJ	ELE	LJ	ELE	LJ	ELE	LJ	ELE	LJ	ELE
0	-6.58	1031.09	-22.53	-2631.61	-25.28	1028.44	-	-	-	-	-	-
0.1	-6.12	1006.37	-21.44	-2580.54	-24.52	1003.89	-13.01	7.99	-17.84	-12.21	-0.17	0.82
0.2	-5.76	981.47	-20.56	-2519.88	-23.45	970.79	-12.04	4.38	-17.05	-16.07	-0.84	0.44
0.3	-5.58	945.63	-18.54	-2450.28	-22.47	941.36	-11.41	2.61	-16.52	-18.11	-0.99	-0.31
0.4	-5.30	905.98	-16.83	-2373.66	-21.66	905.01	-10.02	-1.30	-15.66	-19.94	-1.93	-0.99

<sup>a</sup> A stands for anion and C for cation. All values in  $\text{kJ mol}^{-1}$ .



**Figure 5.** Molar volume,  $V_m$ ,  $\text{CO}_2$  partial molar volume, and liquid phase volume expansion upon  $\text{CO}_2$  absorption for  $x \text{ CO}_2 + (1 - x)$  {[HE3MA]LAC or [3HEMA]MS} systems, at 303 K and 2.5 MPa obtained from molecular dynamics simulations. Symbols: (●) [HE3MA]LAC and (■) [3HEMA]MS mixtures. In panel (a) lines show linear fits, and in panel (b) lines show polynomial fits to the data, for guiding purposes.

a lower ionic liquid expansion upon  $\text{CO}_2$  absorption is obtained for [HMG]LAC than for [HE3MA]LAC, which may be related to the size and shape of the [HMG] cation in comparison with [HE3MA]. Moreover, we should highlight larger  $\text{CO}_2$  solubility in [HMG]LAC than in [HE3MA]LAC, and this confirms the relevance of volumetric effects on  $\text{CO}_2$  absorption. We also report the calculated volume expansion defined according to the Gallagher et al.<sup>40</sup> criterion in Figure 5b, and both fluids show moderate expansion upon  $\text{CO}_2$  absorption, which points to remarkably negative excess molar volumes. To calculate excess molar volume,  $V_m^E$ , we have used the  $\text{CO}_2$  liquid molar volume at 303 K/7.189 MPa ( $73.367 \text{ cm}^3 \text{ mol}^{-1}$ )<sup>41</sup> to obtain values that could be compared with liquid values. Therefore, the estimated  $V_m^E$  values are  $-10.5$  and  $-9.8 \text{ cm}^3 \text{ mol}^{-1}$ , for [HE3MA]LAC and [3HEMA]MA, respectively, both for  $x(\text{CO}_2) = 0.4$ . These large negative excess molar volumes are in agreement with values reported for other families of ionic liquids. Shiflett and

Yokozeki<sup>42</sup> reported a maximum  $V_m^E$  of  $-15 \text{ cm}^3 \text{ mol}^{-1}$  for equimolar mixtures of 1-butyl-methylimidazolium hexafluorophosphate, and Shi and Maginn<sup>15</sup> reported values up to  $-45 \text{ cm}^3 \text{ mol}^{-1}$  for 1-hexyl-3-methylimidazolium bis(trifluoromethylsulfonyl)-imide mixtures. Therefore,  $V_m^E$  for the absorption of  $\text{CO}_2$  in the studied hydroxylammonium ionic liquids are large and negative but lower than for other families of ionic liquids, which is in agreement with the larger partial molar volumes of  $\text{CO}_2$  in hydroxylammonium-based ionic liquid, and that could be related to the moderate solubility of  $\text{CO}_2$  in these fluids.

The low fluid expansion upon  $\text{CO}_2$  absorption may be analyzed also in hydroxylammonium-based ionic liquids considering the void spaces in pure ionic liquids that according to Huang et al.<sup>12</sup> would allow, upon rearrangement, the fit of  $\text{CO}_2$  molecules. Therefore, we report in Figure 6 the distribution of cavity sizes in pure ionic liquids and upon  $\text{CO}_2$  absorption (for  $x(\text{CO}_2) = 0.4$ ), according to the method proposed by Margulis

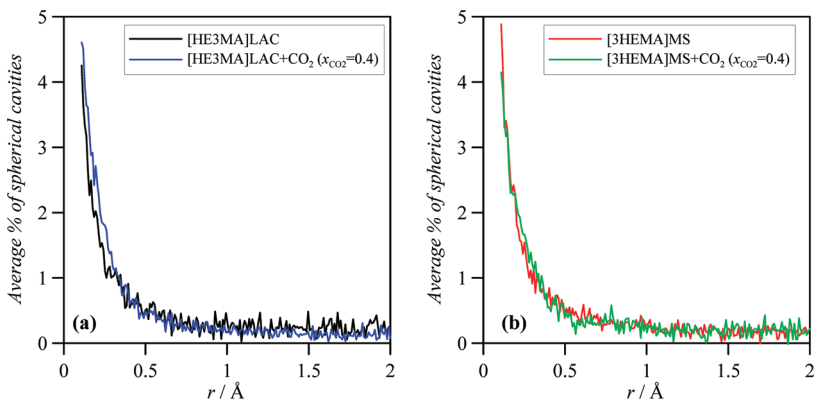


**Figure 6.** Distribution of spherical cavities in pure ionic liquids and in ionic liquids with absorbed  $\text{CO}_2$  at 303 K and 2.5 MPa obtained from molecular dynamics simulations.

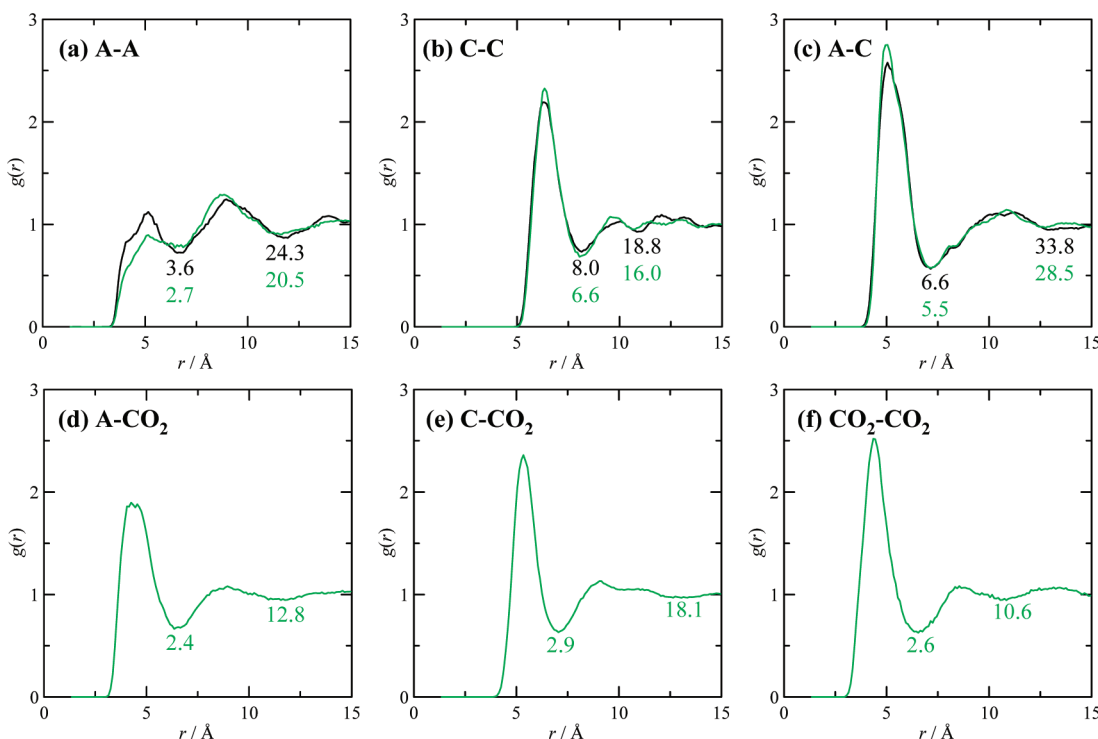


**Figure 7.** Center-of-mass radial distribution functions for pure [HE3MA]LAC (black lines) and for  $x \text{ CO}_2 + (1 - x)$  [HE3MA]LAC mixture at  $x = 0.4$  (green lines), at 303 K and 2.5 MPa obtained from molecular dynamics simulations. A stands for anion and C for cation. Numbers within each panel show the coordination numbers of the first and second solvation shells.

(measuring the smallest distance of random points to all atoms in the liquid).<sup>43</sup> Cavity distributions are very similar for both [HE3MA]LAC and [3HEMA]MS ionic liquids. Moreover, no remarkable changes are inferred for cavity distribution after  $\text{CO}_2$  absorption, only a slight increase of cavities for  $r < 0.4 \text{ \AA}$ . The calculated molecular radius for  $\text{CO}_2$  is  $2.8 \text{ \AA}$ , which is clearly larger than the available cavities in the studied fluids. Therefore, the small volume expansion upon  $\text{CO}_2$  absorption together with the similarities between the cavity distributions for pure and  $\text{CO}_2$ -ionic liquid systems reported in Figure 6 point to cavity rearrangement to explain the  $\text{CO}_2$  absorption mechanism. This was proposed also by Huang et al.<sup>12</sup> and Shi and Maginn<sup>15</sup> for imidazolium-based ionic liquids and by our group for guanidinium-based ones.<sup>36</sup>

**3.3.2. Fluids Structure.** Radial distribution functions, RDFs, for  $x \text{ CO}_2 + (1 - x)$  {[HE3MA]LAC or [3HEMA]MS} and the corresponding integrals are reported in Figures 7–10. Many available computational studies on the structuring of  $\text{CO}_2 +$  ionic liquid mixtures have showed the prevailing role of anion– $\text{CO}_2$  interactions on the  $\text{CO}_2$  absorption, with a more relevant ordering of  $\text{CO}_2$  molecules around anions;<sup>12,44,45</sup> nevertheless, the results obtained in this work for the studied hydroxylammonium-based ionic liquids show that for these fluids both the cation and the corresponding anions have an important role for  $\text{CO}_2$  absorption. Minor changes in RDFs are obtained for both ionic liquids upon  $\text{CO}_2$  absorption. RDFs for anion–anion interactions show the most relevant changes. In the case of [HE3MA]LAC (Figure 7a), the first peak suffers a weakening, and the running

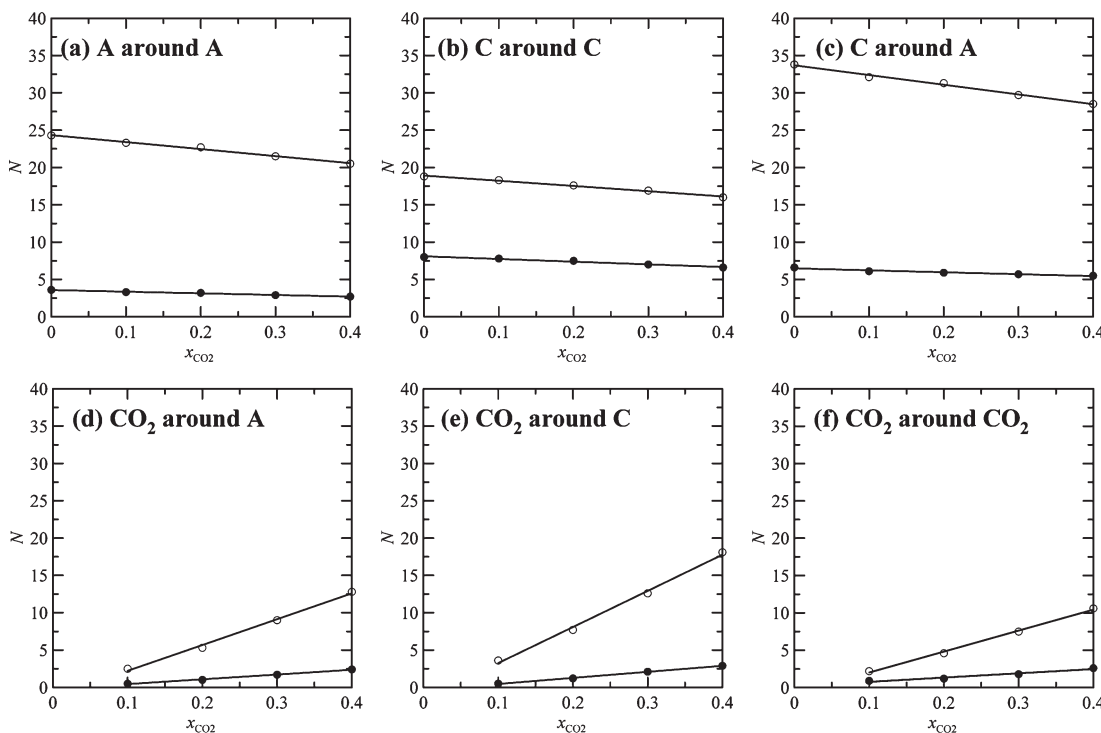


**Figure 8.** Coordination numbers calculated from radial distribution functions for  $x \text{ CO}_2 + (1 - x)$  [HE3MA]LAC mixtures, at 303 K and 2.5 MPa obtained from molecular dynamics simulations. A stands for anion and C for cation. Symbols: first (●) and second (○) solvation shells; continuous lines show linear fits for guiding purposes.

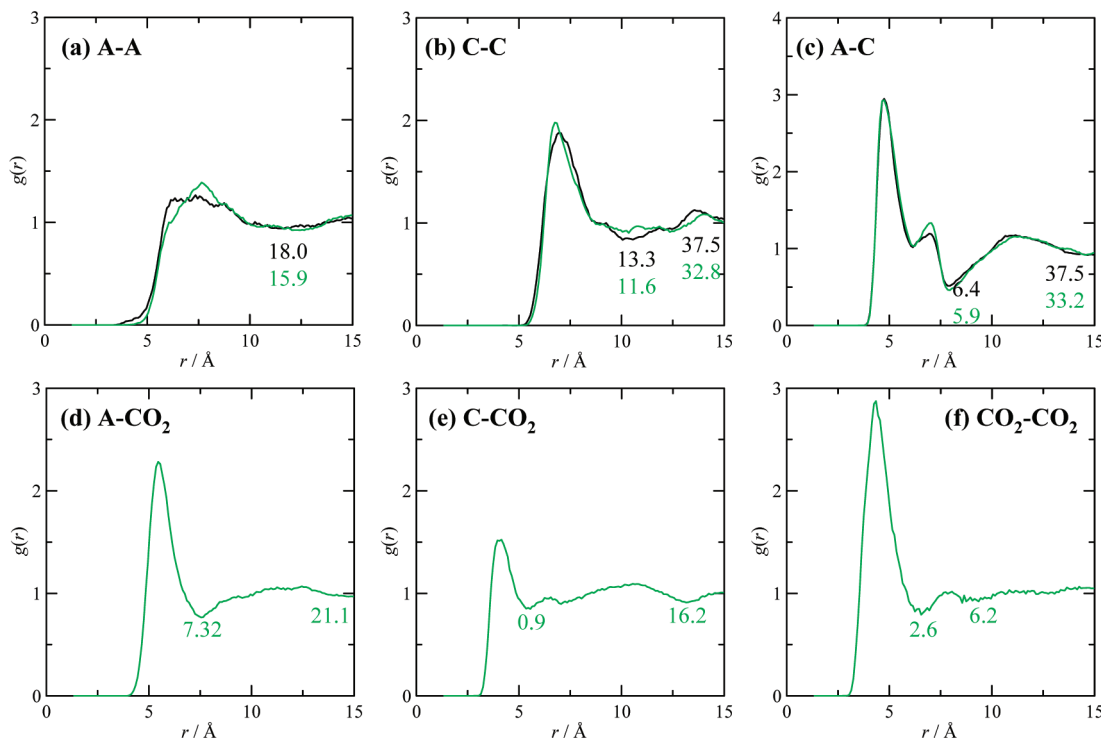


**Figure 9.** Center-of-mass radial distribution functions for pure [3HEMA]MS (black lines) and for  $x \text{ CO}_2 + (1 - x)$  [3HEMA]MS mixture at  $x = 0.4$  (green lines), at 303 K and 2.5 MPa obtained from molecular dynamics simulations. A stands for anion and C for cation. Numbers within each panel show the coordination numbers of the first and second solvation shells.

integrals, for both the first and the second solvation shells (Figure 8a), decrease with increasing CO<sub>2</sub> concentration.

Anion-anion RDF changes are more remarkable for the case of [3HEMA]MS (Figure 9a), for which the wide band in pure

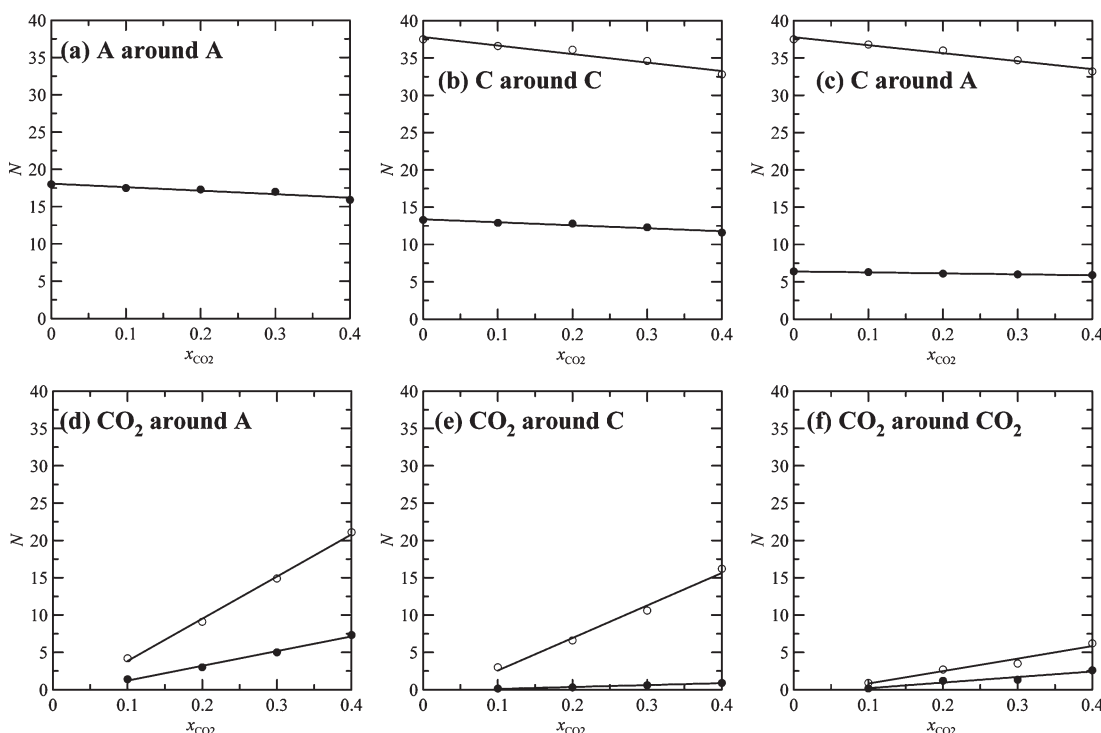


**Figure 10.** Coordination numbers calculated from radial distribution functions for  $x \text{ CO}_2 + (1 - x)$  [3HEMA]MS mixtures, at 303 K and 2.5 MPa obtained from molecular dynamics simulations. A stands for anion and C for cation. Symbols: first (●) and second (○) solvation shells; continuous lines show linear fits for guiding purposes.

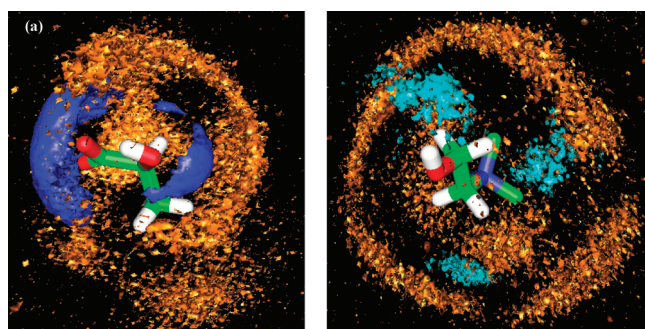


**Figure 11.** Spatial distribution functions of (a) hydroxyl hydrogens in the [HE3MA] cation (H4 atoms, see Table S2, Supporting Information of the previous manuscript in this series)<sup>17</sup> (dark blue surfaces showing 10 times average bulk density) and carbon atoms in CO<sub>2</sub> (orange surfaces showing 5.5 times average bulk density) around the LAC anion. (b) Hydroxyl hydrogens in the lactate anion (H7 atoms, see Table S2, Supporting Information of the previous manuscript in this series)<sup>17</sup> (light blue surfaces showing 10 times average bulk density) and carbon atoms in CO<sub>2</sub> (orange surfaces showing 5.5 times average bulk density) around the [HE3MA] cation. Results obtained from molecular dynamics simulations for the  $x \text{ CO}_2 + (1 - x)$  [HE3MA]LAC mixture at  $x = 0.4$ , 303 K, and 2.5 MPa.

ionic liquid evolves toward a more defined peak; likewise, the integrals (Figure 10a) also decrease with increasing CO<sub>2</sub> concentration. For the case of cation–cation interactions, changes in RDFs are less remarkable despite that both ionic liquids running integrals decrease upon CO<sub>2</sub> absorption as shown in Figures 8 and 10b. The same conclusions are inferred for anion–cation interactions (Figures 8c–10c), and thus a weakening of ion–ion

structuring may be inferred for both ionic liquids, although the reported RDFs show very subtle structural changes produced with CO<sub>2</sub> absorption.

Microscopic distributions of CO<sub>2</sub> around anions and cations (Figures 7d,e–11d,e) show a remarkable structuring around both types of ions. In the case of [HE3MA]LAC, the number of CO<sub>2</sub> molecules around the LAC anion is slightly lower than around the [HE3MA] cation, in the first and especially in the second solvation shell (Figure 8d,e), whereas for [3HEMA]MS the number of CO<sub>2</sub> molecules and the structuring are more remarkable around the MS anion (Figure 10d,e). For the CO<sub>2</sub>–CO<sub>2</sub> interactions (Figures 7f and 10f), a very similar behavior is obtained. In the case of [HE3MA]LAC, a well-defined second shell is obtained (Figure 7f), whereas for [3HEMA]MS this second shell is poorly defined. Thus, a slight preference to solvate the [HE3MA] cation for [HE3MA]LAC and for MS in the case of [3HEMA]MS is inferred, although CO<sub>2</sub> structuring around both types of ions for both ionic liquids is also obtained, but without remarkable changes with CO<sub>2</sub> absorption, which is in agreement with the volumetric results reported in the previous section.

Spatial distribution functions, SDFs, provide a more detailed three-dimensional picture of the structuring in the studied mixed fluids (Figures 11 and 12). SDFs for the cation around the anion in CO<sub>2</sub>/ionic liquid systems (Figures 11a and 12a) are very similar to those reported in the previous work of this series for pure ionic liquids,<sup>17</sup> which is in agreement with the subtle spatial rearrangements upon CO<sub>2</sub> absorption mentioned previously. The distribution of CO<sub>2</sub> around the LAC anion in [HE3MA]LAC is reported in Figure 11a, and results show that CO<sub>2</sub> molecules distribute in a spherical way around LAC excluding the regions in which [HE3MA] cations are preferentially placed (blue caps

around the hydroxyl and carboxylate groups). Moreover, we can see three additional regions that  $\text{CO}_2$  molecules tend to exclude: close to the hydrogen bonded to the central LAC carbon atom, below the methyl LAC group, and the whole region close to the carboxylate group. For the case of the MS anion in [3HEMA]MS (Figure 11a), the distribution of the [3HEMA] cation is almost the same than in the pure fluid, and the arrangement of  $\text{CO}_2$  molecules is almost spherical although less defined than in the case of the LAC anion. The distribution of  $\text{CO}_2$  around the cations is reported in Figures 11b and 12b, and a similar distribution is obtained for both [HE3MA] and [3HEMA] cations:  $\text{CO}_2$  molecules solvating the cations in a spherical way excluding those regions in which LAC and MS anions are placed. Therefore, SDFs show a distribution of  $\text{CO}_2$  molecules in the available void spaces around both cations and anions.

**3.3.3. Energy.** The analysis of interaction energies between the involved species would help to understand the underlying mechanism of  $\text{CO}_2$  absorption. The interaction energies are split

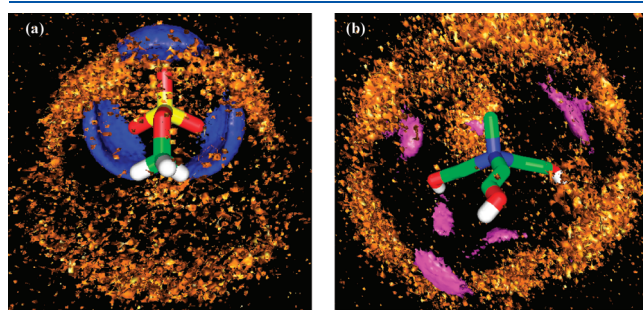


**Figure 12.** Spatial distribution functions of (a) hydroxyl hydrogens in the [3HEMA] cation (H4 atoms, see Table S2, Supporting Information of the previous manuscript in this series)<sup>17</sup> (dark blue surfaces showing 10 times average bulk density) and carbon atoms in  $\text{CO}_2$  (orange surfaces showing 5.5 times average bulk density) around the MS anion; (b)  $\text{SO}_3$  oxygens in the MS anion (O6 atoms, see Table S2, Supporting Information of the previous manuscript in this series)<sup>17</sup> (pink surfaces showing 10 times average bulk density) and carbon atoms in  $\text{CO}_2$  (orange surfaces showing 5.5 times average bulk density) around the [3HEMA] cation. Results obtained from molecular dynamics simulations for the  $x \text{CO}_2 + (1 - x)$  [3HEMA]MS mixture at  $x = 0.4$ , 303 K, and 2.5 MPa. In panel b, hydrogens bonded to carbon atoms are not plotted for the sake of visibility.

into Lennard-Jones (LJ, van der Waals type) and electrostatic (ELE) contributions, and all the individual contributions were analyzed (Table 2). Interionic interaction energies (anion–anion, cation–cation, and anion–cation) are weakened with increasing  $\text{CO}_2$  mole fraction, for both LJ and ELE contributions. LJ interactions are more weakened than ELE contributions (in percentage), although ELE contributions are obviously more important. Moreover, interionic interactions are more weakened in [HE3MA]LAC than in [3HEMA]MS (Table 2). The  $\text{CO}_2$ –ion interactions are characterized by the larger LJ energies in comparison with ELE contributions; nevertheless, for the  $\text{CO}_2$ –cation interactions the ELE contribution is very important, and for the larger  $\text{CO}_2$  mole fractions it is even larger than the LJ terms. We report in Figure 13 a comparison of the total intermolecular interaction energies in the studied ionic liquids. The analysis of the results reported in Figure 13 shows a moderate weakening of total ion–ion interaction energies: 5.3% and 3.2% for [HE3MA]LAC and [3HEMA]MS, respectively. The  $\text{CO}_2$ –ion interaction energies are lower for the [3HEMA]MS than for the [HE3MA]LAC ionic liquid, which would justify the lower absorption ability of the [3HEMA]MS fluid.

**3.3.4. Dynamics.** The dynamic heterogeneity in ionic liquids is a well-known behavior that has been analyzed from theoretical<sup>46–48</sup> and experimental viewpoints.<sup>49,50</sup> This heterogeneity is more remarkable upon  $\text{CO}_2$  absorption: the self-diffusion coefficients,  $D$ , are remarkably larger than those for ions, especially for large  $\text{CO}_2$  mole fractions (Figure 14). All the  $D$  values increase with increasing  $\text{CO}_2$  concentration, which should lead to a decrease in fluid viscosity upon  $\text{CO}_2$  absorption in agreement with the weakening of interionic interaction energies reported in the previous section and with the available measurements for several families of ionic liquids.<sup>51,52</sup> The self-diffusion coefficient is larger for the anion than it is for the cation, for both studied ionic liquids in the studied  $\text{CO}_2$  mole fraction range. For the [HE3MA]LAC ionic liquid, a sudden increase in the self-diffusion coefficients for both anion and cation is produced on going from pure ionic liquid to  $x_{\text{CO}_2} = 0.1$  and then a slight increase with increasing  $\text{CO}_2$  mole fraction (Figure 14a), whereas this effect does not appear for [3HEMA]MS (Figure 14b), which may be justified by the larger size of the [3HEMA] cation. Likewise, the increasing  $D$  values with increasing  $\text{CO}_2$  mole fraction are almost parallel for both the cations and anions, thus pointing to an analogous

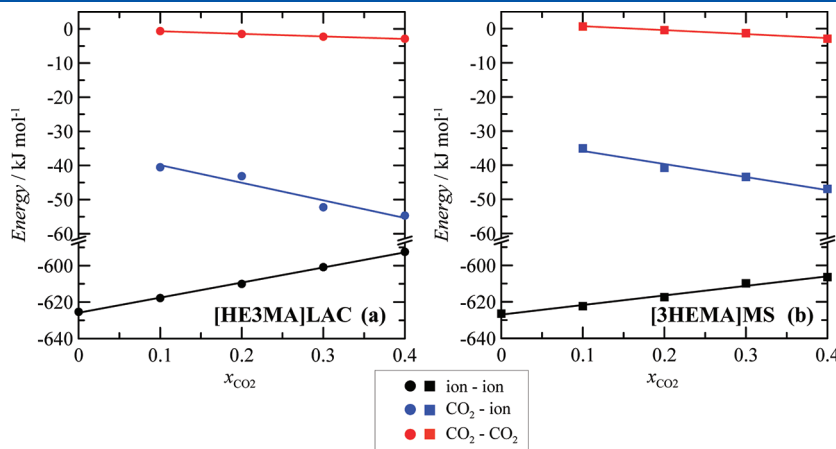


**Figure 13.** Split of intermolecular energies in the liquid phases of  $x \text{CO}_2 + \{(\text{a}) [\text{HE3MA}] \text{LAC or (b)} [\text{3HEMA}] \text{MS}\}$  systems, at 303 K and 2.5 MPa obtained from molecular dynamics simulations. Every term is the sum of Lennard-Jones and electrostatic terms, where ion–ion stands for the sum of anion– $\text{CO}_2$  and cation– $\text{CO}_2$ .

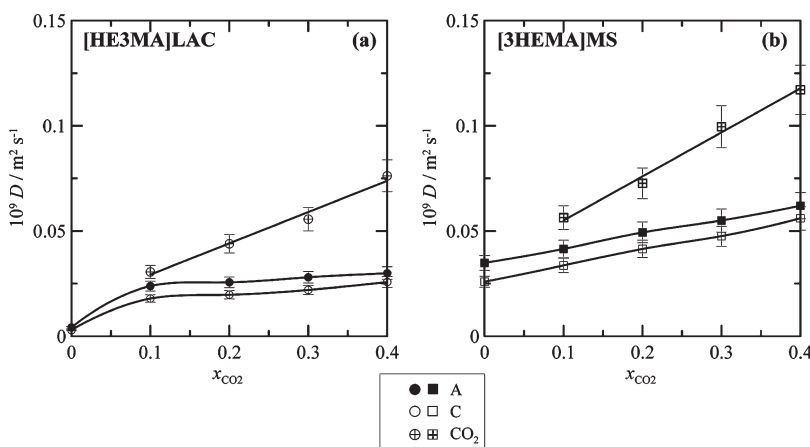


**Figure 14.** Self-diffusion coefficients,  $D$ , for  $x \text{CO}_2 + \{(a) [\text{HE3MA}] \text{LAC} \text{ or } (b) [\text{3HEMA}] \text{MS}\}$  systems, at 303 K and 2.5 MPa obtained from molecular dynamics simulations. A stands for anion and C for cation.

distribution of  $\text{CO}_2$  molecules around both ions. Moreover,  $D$  values for ions in  $[\text{3HEMA}] \text{MS}$  are always larger than for  $[\text{HE3MA}] \text{LAC}$ , in spite of the larger interionic interaction energies reported in Figure 13 for  $[\text{3HEMA}] \text{MS}$ . Self-diffusion coefficients for  $\text{CO}_2$  are remarkably lower than in the bulk supercritical  $\text{CO}_2$  phase,<sup>12</sup> also due to high  $\text{CO}_2$  density, and larger in  $[\text{3HEMA}] \text{MS}$  than in  $[\text{HE3MA}] \text{LAC}$ , which is in agreement with the  $\text{CO}_2$ –ion interaction energies reported in Figure 13. Likewise, the effect of hydroxylammonium cations on the  $\text{CO}_2$  diffusion may be analyzed if the results reported in this work for  $[\text{HE3MA}] \text{LAC}$  are compared with those reported in a previous work for  $[\text{HMG}] \text{LAC}$ .<sup>36</sup> The self-diffusion coefficient for  $\text{CO}_2$  ( $x(\text{CO}_2) = 0.5$ ) in  $[\text{HMG}] \text{LAC}$  is  $0.1265 \times 10^{-9} \text{ m}^2 \text{ s}^{-1}$ , and if results reported in Figure 14a are linearly extrapolated to  $x(\text{CO}_2) = 0.5$  a value of  $0.090 \times 10^{-9} \text{ m}^2 \text{ s}^{-1}$  is obtained. Therefore, a faster  $\text{CO}_2$  diffusion is obtained in  $[\text{HMG}] \text{LAC}$  than in  $[\text{HE3MA}] \text{LAC}$ , and thus the hydroxylammonium cation decreases  $\text{CO}_2$  mobility, which is in agreement with the larger  $\text{CO}_2$ –ion interaction energies reported in this work for  $[\text{HE3MA}] \text{LAC}$  in comparison with those previously reported for  $[\text{HMG}] \text{LAC}$ .<sup>36</sup> Likewise, a certain cooperative effect can be inferred from the comparison of results for  $\text{CO}_2$  in  $[\text{HE3MA}] \text{LAC}$  and  $[\text{HMG}] \text{LAC}$  ionic liquids, and the  $\text{CO}_2$ –LAC interaction energy is clearly lower in  $\text{CO}_2$ – $[\text{HMG}] \text{LAC}$ <sup>36</sup> than in  $\text{CO}_2$ – $[\text{HE3MA}] \text{LAC}$ . Therefore, hydroxylammonium cations lead to strong interactions with  $\text{CO}_2$  molecules, but this effect is combined with very strong anion–cation interactions that lead to not very effective rearrangements of the available void spaces upon  $\text{CO}_2$  absorption (leading to larger  $\text{CO}_2$  partial molar volumes in comparison with other families of ionic liquids) and thus to moderate  $\text{CO}_2$  solubilities.

#### 4. CONCLUDING REMARKS

A wide computational study on the molecular level behavior of hydroxylammonium +  $\text{CO}_2$  systems was performed, under isothermal and isobaric conditions. COSMO predictions of  $\text{CO}_2$  solubility and related properties show the low absorption ability of the studied hydroxylammonium-based ionic liquids. Quantum chemistry analysis of short-range  $\text{CO}_2$ –ion pairs shows not too strong interactions, being stronger with the LAC anion and  $[\text{HE3MA}]$  cation. AIM analysis allowed inferring the characteristics of all the interactions from a topological viewpoint, and the

NBO approach allowed us to analyze the strength of the interactions from the viewpoint of symmetry and energy differences between the donor and acceptor sites. Molecular dynamics simulations of  $\text{CO}_2$ –ionic liquid mixtures showed a very weak effect on the ionic liquid structuring upon  $\text{CO}_2$  absorption, which leads to low  $\text{CO}_2$  partial molar volumes. Nevertheless, these partial molar volumes are larger than values reported in the literature for other ionic liquids with large  $\text{CO}_2$  absorption ability. Spatial distribution of  $\text{CO}_2$  molecules arises from the rearrangement of available void spaces around both cations and anions, thus leading to a moderate weakening of ion–ion interactions and to an increase of molecular mobility that should lead to a decrease in viscosity.

#### ■ ASSOCIATED CONTENT

**S Supporting Information.** Table S1 (systems and conditions used for molecular dynamics simulations). This material is available free of charge via the Internet at <http://pubs.acs.org>.

#### ■ AUTHOR INFORMATION

##### Corresponding Author

\*E-mail: sapar@ubu.es.

#### ■ ACKNOWLEDGMENT

Authors acknowledge the financial support by the Ministerio de Ciencia e Innovación, Spain (Project CTQ2010-15871), and from NPRP grant (No.: NPRP-09-739-2-284) from the Qatar National Research Fund.

#### ■ REFERENCES

- (1) Solomon, S.; Qin, D.; Manning, M.; Chen, Z.; Marquis, M.; Averyt, K. B.; Tignor, M.; Miller, H. L. In *Climate Change 2007: The Physical Science Basis. Contribution of Working Group I to the Fourth Assessment Report of the Intergovernmental Panel on Climate Change*; Solomon, S., Qin, D., Manning, M., Eds.; Cambridge Univ. Press: Cambridge, UK, 2007.
- (2) Baumert, K. A.; Herzog, T.; Pershing, J. *Navigating the Numbers. Greenhouse Gas Data and International Climate Policy*; World Resources Institute: USA, 2005.

- (3) International Energy Outlook Report 2008. DOE/EIA-0484, Energy Information Administration, U.S. Department of Energy, WA, 2008. Available at <http://www.eia.doe.gov/oiaf/ieo/>.
- (4) Figueiro, J. D.; Fout, T.; Plasynski, S.; McIlvried, H.; Srivastava, R. D. *Int. J. Greenhouse Gas Control* **2008**, *2*, 9.
- (5) Desideri, U.; Paolucci, A. *Energy Convers. Manage.* **1999**, *40*, 1899.
- (6) Rao, A. B.; Rubin, E. S. *Environ. Sci. Technol.* **2002**, *36*, 4467.
- (7) Mamun, S.; Svendsen, H. F.; Hoff, K. A.; Juliussen, O. *Energy Convers. Manage.* **2007**, *48*, 251.
- (8) Brennecke, J. F.; Gurkan, B. E. *J. Phys. Chem. Lett.* **2010**, *1*, 3459.
- (9) Hasib, M.; Sajid, M.; Larachi, F. *Chem. Eng. Process* **2010**, *49*, 313.
- (10) Karadas, F.; Atilhan, M.; Aparicio, S. *Energy Fuel* **2010**, *24*, 5817.
- (11) (a) Shiflett, M. B.; Yokozeki, A. *J. Chem. Eng. Data* **2009**, *54*, 108. (b) Pomelli, C. S.; Chiappe, C.; Vidis, A.; Laurenczy, G.; Dyson, P. J. *J. Phys. Chem. B* **2007**, *111*, 13014. (c) Anthony, J. L.; Aki, S. N.; Maginn, E. J.; Brennecke, J. F. *Int. J. Environmental Technol. Manage.* **2004**, *4*, 105. (d) Anthony, J. L.; Crosthwaite, J. M.; Hert, D.; Aki, S. N.; Maginn, E. J.; Brennecke, J. F. In *Ionic Liquids as Green Solvents*; Rogers, R. D., Seddon, K. R., Eds.; American Chemical Society: Washington DC, 2003. (e) Shah, J. K.; Maginn, E. J. *Fluid Phase Equilib.* **2004**, 222–223, 195. (f) Baltus, R. E.; Culbertson, B. H.; Dai, S.; Luo, H.; DePaoli, D. W. *J. Phys. Chem. B* **2004**, *108*, 721. (g) Pérez-Salado, A.; Kamps, D.; Tuma, D.; Xia, J.; Maurer, G. *J. Chem. Eng. Data* **2003**, *48*, 746. (h) Bates, E. D.; Mayton, R. D.; Ntai, I.; Davis, J. H. *J. Am. Chem. Soc.* **2002**, *124*, 926. (i) Anthony, J. L.; Maginn, E. J.; Brennecke, J. F. *J. Phys. Chem. B* **2002**, *106*, 7315. (j) Kumar, P. S.; Hogendoorn, J. A.; Feron, P. H. M.; Versteeg, G. F. *Chem. Eng. Sci.* **2002**, *57*, 1639. (k) Pérez-Salado, A.; Kamps, D.; Tuma, D.; Xia, J.; Maurer, G. *J. Chem. Eng. Data* **2003**, *48*, 746.
- (12) Huang, X.; Margulis, C. J.; Berne, B. J. *J. Am. Chem. Soc.* **2005**, *127*, 17842.
- (13) Gutowski, K. E.; Maginn, E. J. *J. Am. Chem. Soc.* **2008**, *130*, 14690.
- (14) Shim, Y.; Kim, H. *J. Phys. Chem. B* **2010**, *114*, 10160.
- (15) Shi, W.; Maginn, E. J. *Phys. Chem. B* **2008**, *112*, 2045.
- (16) Vega, L. F.; Vilaseca, O.; Llorell, F.; Andreu, J. S. *Fluid Phase Equilib.* **2010**, *294*, 15.
- (17) Aparicio, S.; Atilhan, M.; Alcalde, R.; Fernández, J. *J. Phys. Chem. B* **2011**, DOI: 10.1021/jp2062089.
- (18) Eckert, F.; Klamt, A. *AIChE J.* **2002**, *48*, 369.
- (19) Frisch, M. J.; Trucks, G. W.; Schlegel, H. B.; Scuseria, G. E.; Robb, M. A.; Cheeseman, J. R.; Montgomery, Jr., J. A.; Vreven, T.; Kudin, K. N.; Burant, J. C.; Millam, J. M.; Iyengar, S. S.; Tomasi, J.; Barone, V.; Mennucci, B.; Cossi, M.; Scalmani, G.; Rega, N.; Petersson, G. A.; Nakatsuji, H.; Hada, M.; Ehara, M.; Toyota, K.; Fukuda, R.; Hasegawa, J.; Ishida, M.; Nakajima, T.; Honda, Y.; Kitao, O.; Nakai, H.; Klene, M.; Li, X.; Knox, J. E.; Hratchian, H. P.; Cross, J. B.; Adamo, C.; Jaramillo, J.; Gomperts, R.; Stratmann, R. E.; Yazyev, O.; Austin, A. J.; Cammi, R.; Pomelli, C.; Ochterski, J. W.; Ayala, P. Y.; Morokuma, K.; Voth, G. A.; Salvador, P.; Dannenberg, J. J.; Zakrzewski, V. G.; Dapprich, S.; Daniels, A. D.; Strain, M. C.; Farkas, O.; Malick, D. K.; Rabuck, A. D.; Raghavachari, K.; Foresman, J. B.; Ortiz, J. V.; Cui, Q.; Baboul, A. G.; Clifford, S.; Cioslowski, J.; Stefanov, B. B.; Liu, G.; Liashenko, A.; Piskorz, P.; Komaromi, I.; Martin, R. L.; Fox, D. J.; Keith, T.; Al-Laham, M. A.; Peng, C. Y.; Nanayakkara, A.; Challacombe, M.; Gill, P. M. W.; Johnson, B.; Chen, W.; Wong, M. W.; Gonzalez, C.; Pople, J. A. *Gaussian 03*, revision C.02; Gaussian, Inc.: Wallingford CT, 2004.
- (20) Becke, A. D. *Phys. Rev. A* **1988**, *38*, 3098.
- (21) Lee, C.; Yang, W.; Parr, R. G. *Phys. Rev. B* **1988**, *37*, 7851.
- (22) Becke, A. D. *J. Chem. Phys.* **1993**, *98*, 5648.
- (23) Singh, U. C.; Kollman, P. A. *J. Comput. Chem.* **1984**, *5*, 129.
- (24) Besler, B. H.; Merz, K. M.; Kollman, P. A. *J. Comput. Chem.* **1990**, *11*, 431.
- (25) Simon, S.; Duran, M.; Dannenberg, J. J. *J. Chem. Phys.* **1996**, *105*, 11024.
- (26) Bader, R. F. W. *Atoms in Molecules: a Quantum Theory*; Oxford University Press: Oxford, 1990.
- (27) Biegler-König, F.; Schönbohm, J.; Bayles, D. *J. Comput. Chem.* **2001**, *22*, 545.
- (28) Lyubartsev, A. P.; Laaksonen, A. *Comput. Phys. Commun.* **2000**, *128*, 565.
- (29) Hoover, W. G. *Phys. Rev. A* **1985**, *31*, 1695.
- (30) Tuckerman, M.; Berne, B. J.; Martyna, G. J. *J. Chem. Phys.* **1992**, *97*, 1990.
- (31) Essmann, U. L.; Perera, M. L.; Berkowitz, T.; Darden, H.; Lee, H.; Pedersen, L. G. *J. Chem. Phys.* **1995**, *103*, 8577.
- (32) Ab-Manan, N.; Hardacre, C.; Jacquemin, J.; Rooney, D. W.; Youngs, T. G. A. *J. Chem. Eng. Data* **2009**, *54*, 2005.
- (33) Zhang, X.; Liu, Z.; Wang, W. *AIChE J.* **2008**, *54*, 2717.
- (34) Maiti, A. *ChemSusChem* **2009**, *2*, 628.
- (35) Diedenhofen, M.; Klamt, A. *Fluid Phase Equilib.* **2010**, *294*, 31.
- (36) Aparicio, S.; Atilhan, M. *Energy Fuel* **2010**, *24*, 4989.
- (37) Jacquemin, J.; Husson, P.; Majer, V.; Costa-Gomes, M. F. *Fluid Phase Equilib.* **2006**, *240*, 87.
- (38) Wang, Y.; Wang, C.; Zhang, L.; Li, H. *Phys. Chem. Chem. Phys.* **2008**, *10*, 9776.
- (39) Sudha, S. Y.; Khanna, A. *World Acad. Sci. Eng. Technol.* **2009**, *57*, 539.
- (40) Gallagher, P. M.; Coffey, M. P.; Kruskis, V. J.; Klasutis, N. In *Supercritical Fluid Science and Technology*; ACS Symposium Series, Johnson, K. P., Penninger, J. M. L., Eds.; American Chemical Society (ACS): Washington, D.C., 1989; Vol. 406, Chapter 22, pp 334.
- (41) Lemmon, E. W.; Huber, M. L.; McLinden, M. O. *REFPROP. Reference Fluid Thermodynamic and Transport Properties. NIST Standard Reference Database 23*, version 9.0; U.S. Secretary of Commerce, 2010.
- (42) Shiflett, M. B.; Yokozeki, A. *J. Phys. Chem. B* **2006**, *110*, 14436.
- (43) Margulis, C. *J. Mol. Phys.* **2004**, *102*, 829.
- (44) Bhargava, B. L.; Balasumbramanian, S. *J. Phys. Chem. B* **2007**, *111*, 4477.
- (45) Zhang, X.; Huo, F.; Liu, Z.; Wang, W.; Shi, W.; Maginn, E. J. *J. Phys. Chem. B* **2009**, *113*, 7591.
- (46) Popolo, M. G.; Vath, G. A. *J. Phys. Chem. B* **2004**, *108*, 1744.
- (47) Hu, Z.; Margulis, C. *J. Proc. Natl. Acad. Sci.* **2006**, *103*, 831.
- (48) Yan, T.; Wang, Y.; Knox, C. *J. Phys. Chem. B* **2010**, *114*, 6866.
- (49) Burrell, G. L.; Burgar, I. M.; Gong, Q. *J. Phys. Chem. B* **2010**, *114*, 11436.
- (50) Castigliones, F.; Raos, G.; Appetecchi, G. B.; Montanino, M.; Passerini, S.; Moreno, M.; Famulari, A.; Mele, A. *Phys. Chem. Chem. Phys.* **2010**, *12*, 1784.
- (51) Tomida, D.; Kumagai, A.; Qiao, K.; Yokoyama, C. *J. Chem. Eng. Data* **2007**, *52*, 1638.
- (52) Ahosseini, A.; Ortega, E.; Sensenich, B.; Scurto, A. M. *Fluid Phase Equilib.* **2009**, *286*, 72.